JACS
JOURNAL OF THE AMERICAN CHEMICAL SOCIETY
Article
pubs.acs.org/JACS

Mono-Oxidation of Bidentate Bis-phosphines in Catalyst Activation: Kinetic and Mechanistic Studies of a Pd/Xantphos-Catalyzed C−H Functionalization

Yining Ji,[†] R. Erik Plata,[†] Christopher S. Regens,[‡] Michael Hay,[‡] Michael Schmidt,[‡] Thomas Razler,[‡] Yuping Qiu,[‡] Peng Geng,[‡] Yi Hsiao,[‡] Thorsten Rosner,[‡] Martin D. Eastgate,*[,‡] and Donna G. Blackmond*[,†]

[†]Department of Chemistry, The Scripps Research Institute, 10550 North Torrey Pines Road, La Jolla, California 92037, United States;

[‡]Chemical Development, Bristol-Myers Squibb, One Squibb Drive, New Brunswick, New Jersey 08903, United States

Supporting Information

ABSTRACT: Kinetic, spectroscopic, crystallographic, and computational studies probing a Pd-catalyzed C−H arylation reaction reveal that mono-oxidation of the bis-phosphine ligand is critical for the formation of the active catalyst. The bis-phosphine mono-oxide is shown to be a hemilabile, bidentate ligand for palladium. Isolation of the oxidative addition adduct, with structural elucidation by X-ray analysis, showed that the mono-oxide was catalytically competent, giving the same reaction rate in the productive reaction as the Pd(II)/xantphos precursor. A dual role for the carboxylate base in both catalyst activation and reaction turnover was demonstrated, along with the inhibiting effect of excess phosphine ligand. The generality of the role of phosphine mono-oxide complexes in Pd-catalyzed coupling processes is discussed.

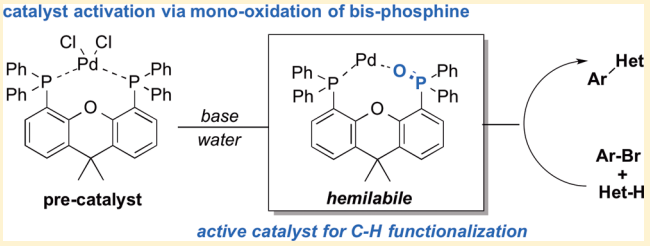

INTRODUCTION

The use of bidentate bis-phosphine ligands is commonplace across metal-mediated transformations including borylation,[1] Suzuki cross-coupling,[2] direct arylation,[3] C−N amination[4] or C−H functionalization.[5] While the main steps of most common catalytic processes are well understood, less knowledge has been gained regarding the entry of the metal/ligand complex into the active cycle. However, this process is critical to the success of the catalyzed reaction, especially for processes involving higher oxidation state metal precatalysts.

Mono-oxides of bis-phosphines have been noted as hemilabile ligands in their own right[6] and have been shown to function in a range of reactions, for example, alkene polymerization,[7] Cu-mediated conjugate reduction,[8] alkyl zinc based conjugate addition,[9] and Pd mediated enantioselective Heck reactions.[10] However, a role for such species has not been considered in reactions employing bidentate bis-phosphines. Herein, we report a detailed kinetic and spectroscopic investigation, including the first solid state characterization, of a xantphos mono-oxide phosphine species in a Pd-mediated C−H functionalization (Scheme 1). The in situ formation of this species from the bisphosphine was found to be key to productive reactivity. Additionally, we elucidate the dual role of base within this transformation. These findings show applicability to other coupling reactions, may contribute to the design of new ligands for more robust catalytic C−H arylation reactions and reveal the importance of precatalyst activation with implications to many coupling processes.

Scheme 1. Pd-Catalyzed C−C Coupling of Imidazole 2 with Pyrrole 1

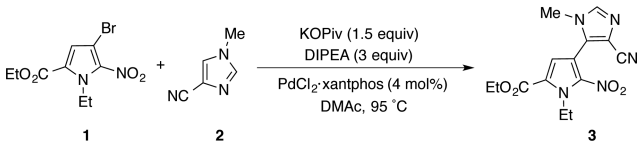

RESULTS AND DISCUSSION

We recently described the significant influence that reduction of a high oxidation state precatalyst can have on the structure of catalytically competent complexes.[11] Our studies showed that even simple changes to the order of addition of key reagents can fundamentally influence both the mechanism of Pd(II) reduction and the structure of the resulting catalytically active complex; for example, in a Miyaura borylation, changing the order of addition resulted in selective formation of either a monoligated or a bis-ligated Pd(0) complex from the same catalyst precursor. We were intrigued by these findings and thus sought to understand their relevance to catalyst activation involving bidentate ligand frameworks in a challenging direct C−H arylation, the coupling of pyrrole **1** to imidazole **2** (Scheme 1). The goal of this study was to gain a comprehensive

Received: February 24, 2015
Published: September 29, 2015

DOI: 10.1021/jacs.5b01913
J. Am. Chem. Soc. 2015, 137, 13272−13281

mechanistic understanding of the reaction, specifically with respect to the process of metal activation and the impact of this process on the resulting catalyst structure.

Ligand screening in the direct arylation of pyrrole **1** found, surprisingly, that the bidentate ligand xantphos[12] was optimal, providing better yields and significantly improved impurity profiles vs monodentate ligands; for example, comparing two $PdCl_2$ precatalyst complexes, xantphos gave a >20% increase in yield when compared to triphenyl phosphine (see Supporting Information). The yield improvement with xantphos was attributed to a significant decrease in the number of side products.

Recent experimental and computational studies on the direct C−H arylation of unactivated substrates have delineated mechanisms for the C−H bond cleavage step,[13] including proposals for both an electrophilic aromatic substitution (SEAr)[14] and a concerted metalation−deprotonation (CMD).[15] CMD has been the generally accepted mechanism, where the base acts as an anionic ligand on the catalytic metal center mediating the proton abstraction required for productive coupling,[16] with pivalate salts the preferred choice.[17] In the accepted CMD pathway, an open site for coordination on the metal center is generally proposed, though other suggestions have been made.[3a]

These findings pose an important question for the transformation in Scheme 1: with the accepted mechanism for a CMD process, how can a bidentate ligand function in this coupling process? At first inspection it appears that the metal center would be forced into a congested penta-coordinate transition state for the CMD step (Scheme 2). One might suggest

Scheme 2. CMD Coupling of Pyrrole 1 and Imidazole 2 in the Absence of Ligand Dissociation Would Involve an Unlikely Penta-Coordinated Transition State

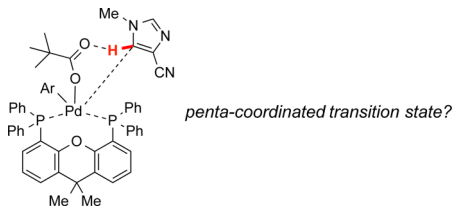

deligation of one phosphine, but this potential requirement would suggest that a bidentate ligand framework would be inferior to a monodentate ligand (such as triphenylphosphine); however, our results show that this is not the case. We therefore interrogated this reaction in some detail, starting with a kinetic analysis.

Kinetic Analysis. Our optimized conditions for the formation of biaryl **3** employed a homogeneous, dual base system of potassium pivalate (KOPiv), which is crucial for productive reaction, and Hünigs base (employed to avoid buffering at high conversion). Reaction Progress Kinetic Analysis (RPKA)[18] of the temporal concentration profiles allows kinetic dependences to be determined with a minimal number of carefully designed experiments.

The results of experiments carried out using the "different excess" protocol are shown in Figure 1.[19] Comparison of the slopes of reaction profiles plotted for [**2**] as a function of time for reaction with the same $[\mathbf{2}]_0$ and different values of $[\mathbf{1}]_0$ reveals the concentration dependence of pyrrole **1**; the converse set of experiments with the same $[\mathbf{1}]_0$, different $[\mathbf{2}]_0$, gives the dependence on [**2**]. Overlay between the profiles in

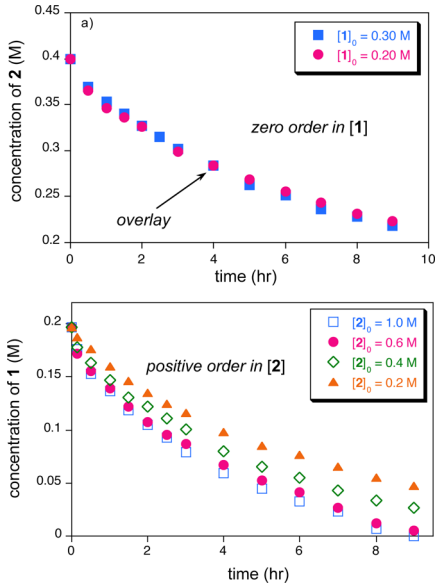

Figure 1. Temporal concentration profiles monitored by NMR spectroscopy for the reaction of Scheme 1 carried out under "different excess" protocol for determining orders in [**1**] and [**2**]. [$PdCl_2$·xantphos] = 0.008M; [KOPiv] = 0.3 M; [DIPEA] = 0.6 M; (a) $[\mathbf{2}]_0$ = 0.4 M, $[\mathbf{1}]_0$ as noted; (b) $[\mathbf{1}]_0$ = 0.2 M, $[\mathbf{2}]_0$ as noted. Reaction time ca. 8−10 h.

Figure 1a reveals zero-order kinetics in [**1**]. The difference in slopes of temporal concentration profiles for the reactions in Figure 1b, with the higher concentration of **2** giving faster rates, indicates a positive order in [**2**]. At higher concentrations of **2**, the profiles nearly overlay, suggesting saturation kinetics in [**2**]. Typical reaction times under these conditions are 8−10 h.

The reaction gives first-order dependence on the concentration of the catalyst precursor ($PdCl_2$·xantphos, see Supporting Information). However, the lack of overlay in the time-adjusted "same excess" protocol (Figure 2) reveals either catalyst

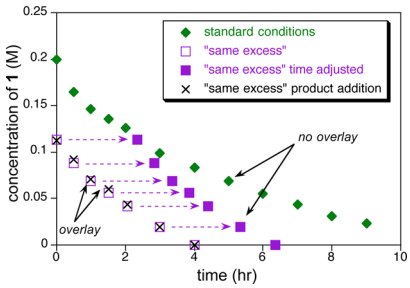

Figure 2. "Same excess" and product addition experiments in the reaction of Scheme 1 carried out using [$PdCl_2$·xantphos] = 0.008 M; [DIPEA] = 0.6 M; [KOPiv] = 0.3 M. Standard conditions: $[\mathbf{1}]_0$ = 0.2 M, $[\mathbf{2}]_0$ = 0.6 M, (excess = 0.4 M). "Same excess" conditions: $[\mathbf{1}]_0$ = 0.12 M, $[\mathbf{2}]_0$ = 0.52 M. Same excess, product addition conditions: $[\mathbf{1}]_0$ = 0.12 M, $[\mathbf{2}]_0$ = 0.52 M, $[\mathbf{3}]_0$ = 0.08 M.

deactivation or product inhibition. No evidence of product inhibition was observed during product addition experiments, suggesting that other processes are responsible for the lack of reaction profile overlay. Additional experiments indicated zero-order relationships for both KOPiv and Hünigs base DIPEA (see Supporting Information). Interestingly, despite the fact that reaction rate is not influenced by the concentration of KOPiv itself, the reaction is sensitive to the nature of the

DOI: 10.1021/jacs.5b01913
J. Am. Chem. Soc. 2015, 137, 13272−13281

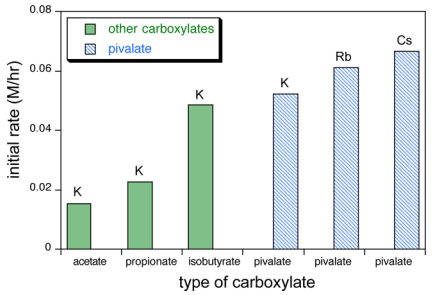

Figure 3. Initial rates for the reaction of Scheme 1 carried out using different carboxylate bases [$PdCl_2$·xantphos] = 0.008 M; $[\mathbf{1}]_0$ = 0.2 M, $[\mathbf{2}]_0$ = 0.6 M, [base] = 0.5 M.

carboxylate species (Figure 3), which is consistent with a CMD mechanism. For example, as the steric bulk is increased from potassium acetate to the corresponding pivalate, an increase in reactivity (reaction rate) is observed, even while zero-order kinetics is maintained in the kinetic profiles of reactions carried out with each base; similar behavior of carboxylates bases on a palladium-catalyzed arylation have been reported.[17a] The pivalates with counterions potassium, rubidium and cesium performed similarly, with a slight increase in initial rate across the series. These results suggest a complex role for the carboxylate base.

Kinetic Isotopic Effect (KIE). Kinetic isotope measurements were carried out using imidazole **2**-D, deuterated in the C5-position, both under competition conditions (in one flask), and in parallel experiments (in separate flasks), as shown in Figure 4a.[30] Both protocols show a normal KIE, of magnitude

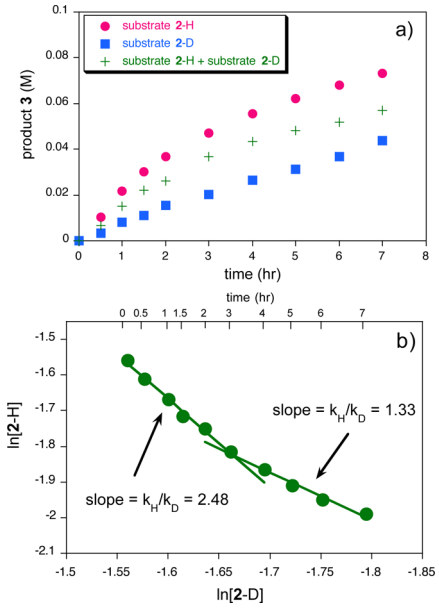

Figure 4. (a) Temporal product concentration profiles monitored by NMR spectroscopy for the reaction carried out by using H- and D-imidazole **2** in separate reactions (red circles and blue squares) or in competition (green plus symbols); (b) ln[**2**-H] vs ln[**2**-D] from the data in (a) over the course of the reactions carried out in separate flasks. The upper *x*-axis indicates the time of each data point from the runs in (a).

k_H/k_D = ca. 2.4 from initial rates in the parallel reactions and k_H/k_D = ca. 1.4 from product ratios at extended reaction time in the competitive case. This difference may be rationalized by considering the complex catalytic rate behavior in this reaction, as manifested by the observation of saturation kinetics in [**2**]. Because saturation kinetics dictates that the reaction order in [**2**] shifts over the course of the reaction, at a given time during the competitive reaction, the rate dependence for the more rapidly reacting **2**-H may shift from zero-order toward first-order even while the slower reacting **2**-D remains zero-order, resulting in a changing ratio of rates.

The effect of saturation kinetics on KIE can be quantified by comparison to the general case of first-order kinetics (eq 1, see Supporting Information for derivation). The value of the KIE = k_H/k_D obtained for reactions following first-order kinetics from the slope of a plot of ln[**2**-H] vs ln[**2**-D] gives a straight line, as shown in eq 1. However, plotting the data from Figure 4a in this form in Figure 4b reveals that the slope, and hence the KIE, changes over the course of the reaction. This supports the idea that the reaction exhibits a rate law more complex than simple first-order kinetics.

$$\ln[\mathbf{2}\text{-H}] = \left(\frac{k_H}{k_D}\right)\cdot\ln[\mathbf{2}\text{-D}] \quad (1)$$

The KIE measured from the product ratio in the competitive reaction is in good agreement with the value found at high conversion in the parallel experiments, while the value taken from the separate experiments is in agreement with the initial slope of Figure 4b. Both protocols indicate a moderate normal kinetic isotope effect, which suggests that the C−H activation step is not solely rate-determining. The observed shift in KIE values with reaction progress is in accordance with the kinetic finding of saturation kinetics in [**2**], suggesting that reversible addition of **2** to a catalyst complex precedes an irreversible step involving C−H activation.

Identification of Catalytic Intermediates. We attempted to identify Pd species via ^{31}P NMR spectroscopy by analyzing interactions between the Pd/xantphos precatalyst with each of the reaction components, alone and in combination. No changes were observed between the preformed $PdCl_2$·xantphos complex and pyrrole **1**, nor with addition of either DIPEA or imidazole **2**, after heating to 95 °C (Figure 5). However,

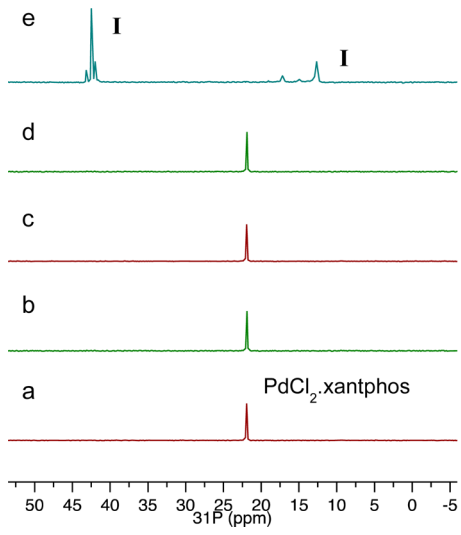

Figure 5. A 202 MHz ^{31}P NMR spectra showing (a) $PdCl_2$·xantphos; (b) $PdCl_2$·xantphos and **1**; (c) $PdCl_2$·xantphos, **1**, and **2**; (d) $PdCl_2$·xantphos, **1**, and DIPEA; (e) $PdCl_2$·xantphos, **1**, and KOPiv. All spectra recorded in DMAc-d_9 at ambient temperature.

DOI: 10.1021/jacs.5b01913
J. Am. Chem. Soc. 2015, 137, 13272−13281

contact between $PdCl_2$·xantphos and pyrrole **1** in the presence of KOPiv resulted in formation of new species **I** (with two phosphorus resonances at 12.8 and 42.6 ppm).

Stoichiometric reaction between $PdCl_2$·xantphos, **1**, and KOPiv enabled a species to be isolated as an air-stable yellow solid that showed no noticeable decomposition on standing. The complex dissolved in DMAc-d_9 gives the same ^{31}P NMR spectrum as **I** (Figure 5e). The structure of the complex was established by X-ray diffraction (Figure 6) and determined to

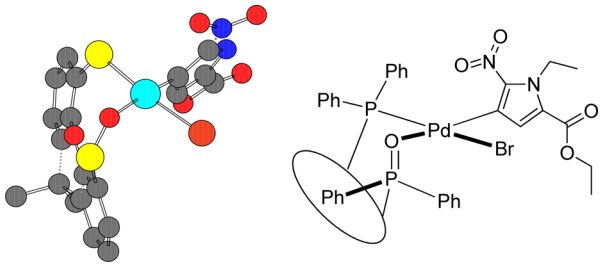

Figure 6. X-ray structure of complex **I·Br** (left) and chemdraw representation (right). Noncritical H and C atoms removed for clarity Pd = turquoise, P = yellow, C = gray, Br = brown, O = red.

be the oxidative addition complex of **1** to $PdCl_2$·xantphos, designated **I·Br**, in which, notably, one of the phosphorus atoms has been oxidized. To the best of our knowledge, the identification of complex **I·Br** is the first report of such a xantphos mono-oxide complex of Pd in the solid state. Bidentate mono-oxide metal complexes with other bis-phosphines showing evidence of P═O—M bonding have been characterized previously. As early as 1983 White et al. established the structure of *o*-[C_6H_4(PMePh)(P(O)MePh)] bound to Ru;[20] several other metals have since been observed in mixed bidentate P/PO complexes (for example Hg,[21] Mo,[22] Cu,[23] Pt[24] and Os).[25] However, limited examples of Pd complexation with bis-phosphine mono-oxides have been reported.[26]

The crystal structure shows that the xantphos mono-oxide ligates the palladium as a chelate, with the phosphine-oxide oxygen coordinated directly to the metal. This binding mode enables the Pd to move out of the plane of the xantphos backbone, with the ligand architecture moving slightly under the ligand sphere. The pyrrole **1** sits trans to the phosphine oxide, with the bromide trans to the phosphine. It is important to note in this structure that complexation of the xantphos mono-oxide has a much smaller bite angle than the parent bis-phosphine.

I·Br treated with the parent xantphos (bis-phosphine) shows displacement of the mono-oxide to new species, **II** and **IV** (Figure 7a). Species **II** was assigned as the displaced mono-oxide of xantphos by comparison to an authentic sample (Figure 7b).[27] Species **II** is unstable in air and was found to undergo further oxidation to the bis-oxide **III** (Figure 7c). Species **IV** was assigned by X-ray diffraction as the bidentate oxidative addition complex of substrate **1** and xantphos. In addition, **IV** could be prepared independently from $Pd_2(dba)_3$, xantphos and **1** (see Supporting Information). Scheme 3 outlines the formation of these species from **I·Br**.

Complex **I·Br** remains unchanged when heated in solution to reaction temperature in the absence of KOPiv, and reaction with **2** does not proceed in the absence of KOPiv under either stoichiometric or catalytic conditions. Stoichiometric reaction of **I·Br** with **2** and KOPiv proceeds smoothly to product **3** (see Supporting Information). Employing complex **I·Br** in the

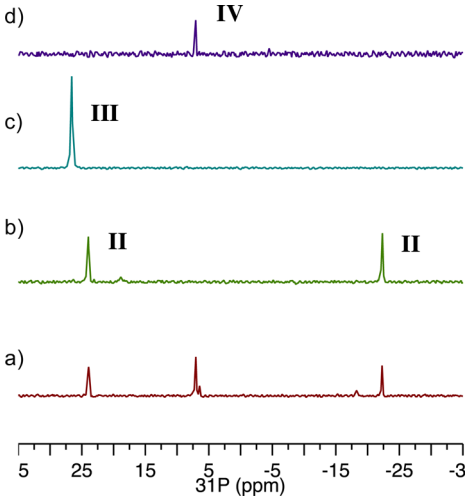

Figure 7. A 202 MHz ^{31}P NMR spectra of (a) complex **I·Br** in the presence of excess xantphos ligand; (b) xantphos mono-oxide **II**; (c) xantphos bis-oxide **III**; (d) oxidative addition complex of substrate **1** with xantphos, **IV**. All the spectra were recorded in DMAc-d_9.

Scheme 3. Interaction of Intermediate I·Br with Xantphos

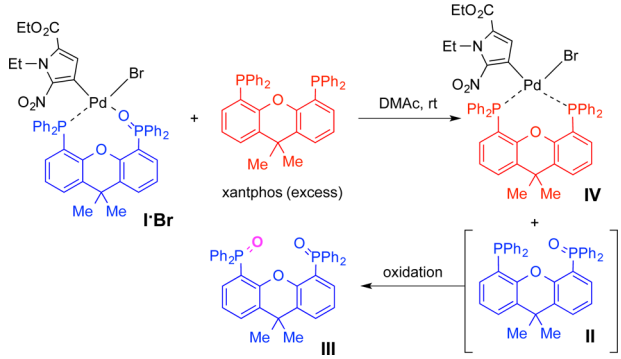

coupling reaction under catalytic conditions revealed, strikingly, that **I·Br** was equally effective as $PdCl_2$·xantphos used as precatalyst (Figure 8). The lack of an induction period using

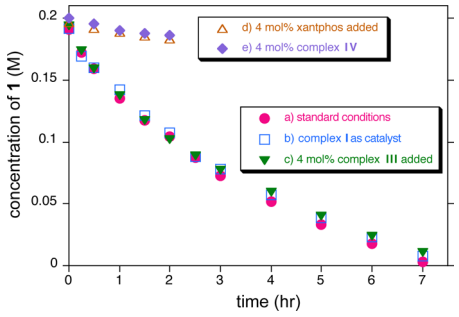

Figure 8. Kinetic profiles for the reaction of Scheme 1. (a) Standard conditions with 4 mol % $PdCl_2$·xantphos as catalyst precursor; (b) standard conditions with 4 mol % complex **I·Br** as catalyst; (c) standard conditions with 4 mol % $PdCl_2$·xantphos and 4 mol % **III**; (d) standard conditions with 4 mol % $PdCl_2$·xantphos and 4 mol % xantphos; (e) standard conditions with 4 mol % **IV**.

I·Br in place of $PdCl_2$·xantphos supports its competence in the catalytic cycle. Interestingly, the reaction failed when the bisphosphine complex **IV** was employed. Addition of excess free xantphos bis-phosphine to the standard reaction also

DOI: 10.1021/jacs.5b01913
J. Am. Chem. Soc. 2015, 137, 13272−13281

significantly inhibited the coupling, while addition of the xantphos bis-oxide **III** had no influence on reaction rate (Figure 8). These results suggest that the binding strength to Pd is in the order xantphos > **II** ≫ **III**.

We observed species **I** in samples of the catalytic reaction mixture cooled to ambient temperature (Figure 9). During

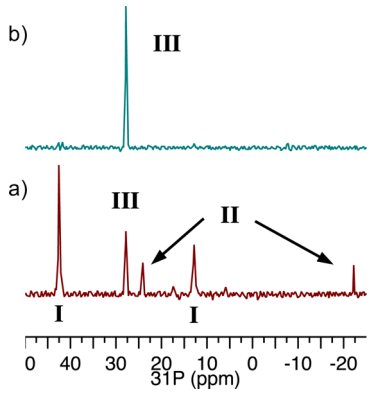

Figure 9. A 202 MHz ^{31}P NMR spectra of aliquots taken (a) during the reaction of Scheme 1 (30 min); (b) after reaction (16 h). All the spectra were recorded in DMAc-d_9 after cooling to room temperature.

the reaction, species **II** and **III** also appear. As the reaction progresses, **III** increases at the expense of **I** and **II**, with **III** being the only species detected at the end of the reaction. This suggests that formation of the bis-phosphine oxide **III** may be related to the observed catalyst decomposition.

Role of the Base. Scheme 4 probes the complex role of base in this transformation. Species **I·Br** requires base for its

Scheme 4. Role of Bases in the Reaction of Scheme 1

base	"Step A" competent to form I·Br	"Step B" competent to form 3 from I·Br
KOPiv	yes	yes
K-acetate	yes	yes
KO^{t}Bu	yes	no
KOEt	yes	no
K-phthalimide	no	no
DIPEA	no	no

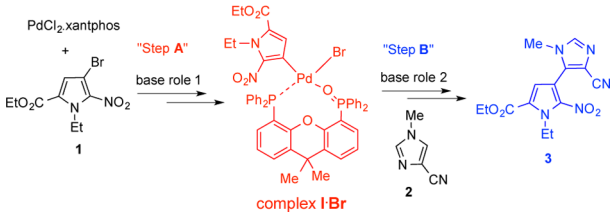

formation from $PdCl_2$·xantphos and **1**, which occurs in the presence of KOPiv, K-acetate, KO^{t}Bu, and KOEt, but not in the presence of amidates or amines. This suggests a role for the former bases in promoting reduction of the stable Pd(II) precursor and concomitantly oxidizing the ligand. This would be consistent with previous reports, where base and adventitious water were shown to reduce Pd(II) to Pd(0) with concurrent phosphine oxidation.[28] Scheme 4 shows that under stoichiometric conditions, **I·Br** reaction with imidazole **2** failed to produce product **3** in the presence of noncarboxylate bases. Thus, bases may be characterized by their ability to mediate two important steps in the process—catalyst activation, leading to the formation of intermediate **I·Br** ("Step **A**" in Scheme 4) and/or their ability to mediate the productive coupling events, to product **3** ("Step **B**").

The observed zero-order kinetics in base concentration and saturation kinetics in [**2**] suggests that a species formed subsequent to base addition to **I·Br** represents the resting state under high temperature catalytic conditions. NMR studies of complex **I·Br** after heating to reaction temperature in the presence of KOPiv provide support for an ion-exchange process between Br and OPiv. Figure 10 shows that two new features

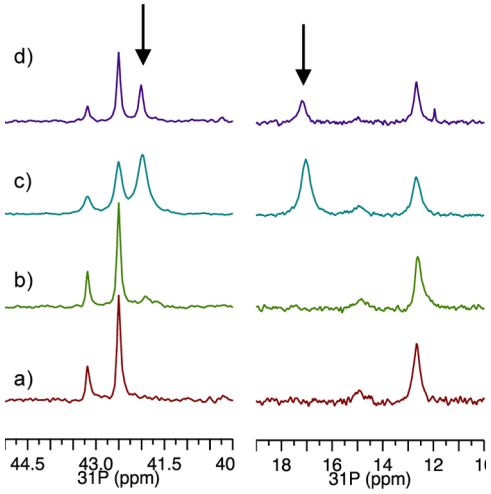

Figure 10. A 202 MHz ^{31}P NMR spectra of complex **I·Br** (0.033 M) at ambient temperature in DMAc-d_9 after heating to 95 °C (a) in the absence of KOPiv; (b) with 0.066 M KOPiv; (c) with 1.2 M KOPiv; (d) during reaction with **2** (0.2 M) and KOPiv (0.4 M).

appear in the ^{31}P NMR spectrum (marked with arrows) upon heating of complex **I·Br** with increasing amounts of KOPiv, features that are also observed under catalytic turnover. A ^{13}C NMR experiment of complex **I·Br** in the presence of KOPiv showed a new peak not present in the spectra of either species alone. This was assigned to a quaternary carbon by a DEPTQ experiment (distortionless enhancement by polarization transfer with retention of quaternaries), which we attribute to the pivalate bound to Pd (see Supporting Information). Together these studies suggest that counterion exchange between the original oxidative addition complex **I·Br** and KOPiv yields the catalytic resting state of the oxidative addition complex of **1** with pivalate ligand, denoted as **V**. Such exchange processes between Pd carboxylates and other ligands including halides are well documented.[29]

Computational Modeling. Computational studies of the potential reaction coordinate were carried out to help understand this reaction in more detail, especially the role of the ligand mono-oxide. This study was performed using the B3LYP density functional theory (DFT) method through the Gaussian suite of programs.[31] We first compared several basis-sets and their ability to replicate the crystal structure of the mono-oxide complex **I·Br**; the same basis-set was used for all atoms, with effective core potential (ECP) only for Pd. The calculated bond-lengths were then compared to the crystal structure; the differences in key bond-lengths are shown (Table 1). On the basis of this analysis, defSV(P)[32] provided the best approximation across all key bonds and thus we used defSV(P) for the analysis of the entire reaction coordinate.[33] M06 has shown some benefit for assessing ligand—metal binding energies in

DOI: 10.1021/jacs.5b01913
J. Am. Chem. Soc. 2015, 137, 13272−13281

Table 1. Data Comparing the Key Bond-Lengths for the Crystal Structure of Complex I·Br to Those Calculated by defSV(P), DZVP,[35] CEP-121,[36] and PM6[37a]

delta (Å)	P−Pd	P═O−Pd	Br−Pd	C−Pd
defSV(P)	**0.103**	**0.066**	**0.027**	**0.038**
DZVP	0.161	0.097	0.052	0.062
CEP-121	0.191	−0.002	0.071	0.049
PM6	−0.007	0.329	0.066	−0.031

[a]Values are defined from $BL_{calc} - BL_{X\text{-}ray}$.

ruthenium mediated metathesis processes;[34] thus, all structures described below were also analyzed at M06/defSV(P). In this study, B3LYP gave the most consistent results to experimental observations; PCM solvent compensation (DMAc) was also assessed, providing a similar energy profile though inconsistent C5/C2 selectivities (see Supporting Information). Thus, B3LYP/defSV(P) without solvent correction was employed.

We explored intermediates aligned with the typical mechanism associated with C−H functionalization, namely Fagnou's proposed CMD mechanism,[17] with thermal free energies (at 298 K) being evaluated. We first confirmed the conclusion reached from the kinetic data that the pivalate complex serves as the resting state by analyzing computationally the conversion between complex **I.Br** and complex **V** via their hydrated potassium salts (see Supporting Information). Calculations using B3LYP/defSV(P) with PCM/DMAc showed that the conversion is slightly endothermic. Under reaction conditions, where the concentration of KOPiv is in excess of the total [Pd] typically by 3 orders of magnitude, this translates to >95% of the total Pd being present as complex **V**. And while the fraction of **V** is predicted to decrease as KOPiv is consumed and bromide builds up over the course of reaction turnovers, the low solubility of KBr limits the extent of the shift back to **I.Br**. **V** remains the dominant species, confirming the kinetic proposal of **V** as the resting state during catalysis. Therefore, we started our computational study after this displacement.[17] All energies are relative to complex **V**, the product of pivalate displacement on complex **I.Br**.

Significant steric constraints inhibit the forward reaction of **V** without the opening of one coordination site on the metal center along with a potential ligand rotation. However, it was unclear how the rigid xantphos ligand would be able to act in this way. One possible pathway involves the phosphine oxide of the xantphos mono-oxide acting in a hemilabile manner, creating an open site for complexation of reactants. A similar function in the bis-phosphine mono-oxide bozPHOS has been proposed.[38] We considered that the displacement of the phosphine oxide by the Pd-bound pivalate of complex **V**, forming the bidentate pivalate complex **VI**, may occur (Scheme 5). A viable transition state for this displacement was quickly found, which appeared more similar to a Berry pseudo rotation than an associative displacement.[39] Thus, association of the carbonyl oxygen with palladium, followed by a transition-state involving ligand movement around a trigonal-bipyramid, resulted in the phosphine oxide being displaced from the metal center. The transition-state energy for this displacement was at 9.6 kcal mol^{-1} relative to the initial Pd(II) complex **V**, producing the bridged carboxylate complex **VI**.[40] The P═O displacement resulted in the phosphine oxide sitting under the coordination plane of the metal center with a PO-Pd distance of 2.92 Å (Figure 11). To create a suitable steric environment for the subsequent steps, it appeared that ligand rotation was required, placing the phosphine oxide

Scheme 5. Berry Pseudo Rotation Mechanism for Xantphos Mono-oxide Displacement

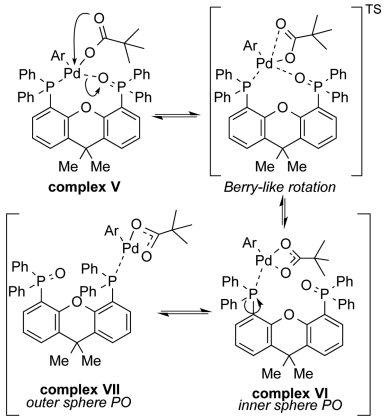

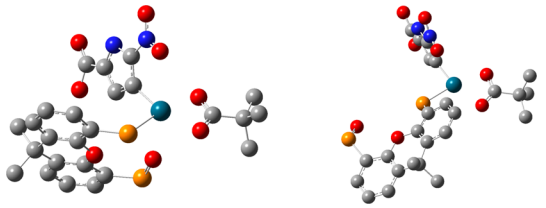

Figure 11. Inner sphere **VI** (left) and outer sphere **VII** (right) P═O geometries. Noncritical H and C atoms removed for clarity. Carbon = gray, oxygen = red, phosphorus = yellow; nitrogen = blue, palladium = turquoise.

external to the ligand field, complex **VII**. While no formal transition state was investigated for this rotation, an energy scan was performed at PM6, rotating the xant-P bond (Scheme 5). This scan suggested a rotational energy of ∼16 kcal mol^{-1} from the intermediate complex **VI**.

With an open coordination site on Pd, ligation of imidazole **2** gave an N3-bound complex as the lowest energy isomer (9.2 $kcalmol^{-1}$) relative to the starting complex and 2.7 kcal mol^{-1} higher than the bridged pivalate intermediate (Figure 12).

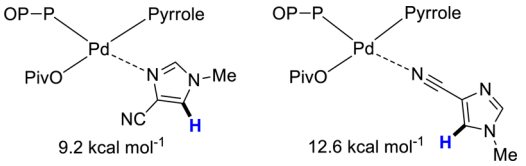

Figure 12. Orientations for binding of imidazole **2** to the metal center. Coordination through the nitrile would enable the desired C−H to be accessible for functionalization.

An alternate complex with the −CN nitrogen bound to the Pd (12.6 kcal mol^{-1}) was also observed. This is likely to be the more reactive confirmation given the proximity of the C5-proton to the metal center. The solvent, DMAc, was found to act as a ligand for palladium, in a fashion similar to the imidazole, though forming a less stable complex (ca. 13.3 kcal mol^{-1}).

The transition-states for the CMD event, leading to the C5 and C2 isomers of the coupled product, were identified; transition-state energies of 30.6 and 31.4 kcal mol^{-1} (C5/C2, respectively) were consistent with the observed selectivity preference[41] and previous reports (Figure 13).[42] The mechanism of pivalate departure was not interrogated in detail, though direct dissociation to a tricoordinate intermediate was assessed. The

DOI: 10.1021/jacs.5b01913
J. Am. Chem. Soc. 2015, 137, 13272−13281

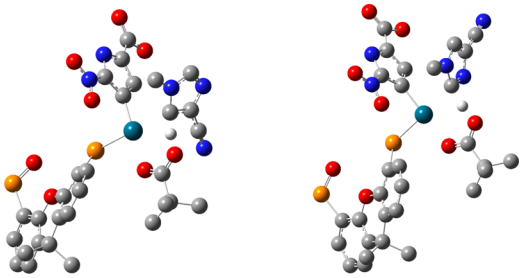

Figure 13. Transition-states for the lowest energy C5 (left) and C2 (right) CMD processes. Noncritical H and C atoms removed for clarity.

tricoordinate species is higher in energy than the CMD metalation (ca. 34 kcal mol^{-1}), inconsistent with the observed kinetics. Rebinding of the hemilabile phosphine oxide resulted in a complex of only 9.1 kcal mol^{-1}, suggesting that rotation and recoordination of the phosphine oxide is linked to pivalate departure (Scheme 6).

Scheme 6. Proposed Process for Pivalic Acid Displacement from Pd

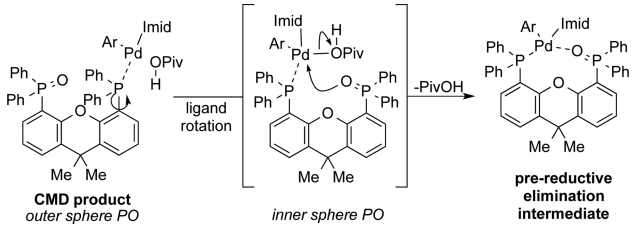

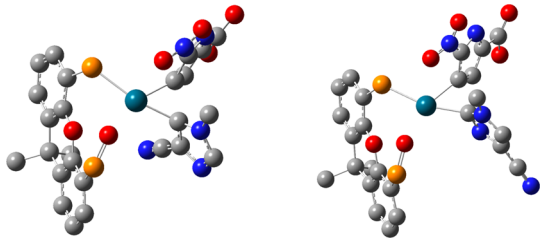

Figure 14. Transition-states for reductive elimination C5 (left) and C2 (right). Noncritical H and C atoms removed for clarity.

Reductive elimination proceeded from both regio-isomeric complexes with approximately identical transition-state energies (ca. ∼26 kcal mol^{-1}); these energies are lower than the CMD, suggesting that the CMD is turnover limiting, consistent with the kinetic analysis. The transition-states for reductive elimination had C−C distances for the forming bonds similar to those reported, 1.84 and 1.83 Å, respectively, with C−Pd−C angles of 53.2° and 52.7° (Figure 14).[43]

The thermal free energy profile for the reaction coordinate is shown (Figure 15). The computational study revealed several important factors: (a) ligand dissociation and rotation are likely required for productive reaction; (b) ligand rotation is a high energy process, close in energy to the turnover limiting transition-states; (c) the initial imidazole bound complex is likely not a productive intermediate, with imidazole ligand exchange potentially being required; (d) the CMD is likely turnover limiting and C5 selective, consistent with the kinetic analysis. Importantly, these studies confirmed the importance of ligand mono-oxidation to enable the hemilabile functionality of xantphos.

Mechanistic Proposal. The experimental kinetic, spectroscopic, and structural data together with the computational analysis lead to proposal of the catalytic reaction mechanism shown in Scheme 7. Precatalyst reduction is concomitant with phosphine oxidation and is mediated by base (under these conditions KOPiv), producing the Pd(0)·xantphos mono-oxide complex on the catalytic cycle, which then undergoes oxidative addition to the aryl halide to produce **I·Br**. After anionic ligand exchange of Br with pivalate to form **V**, displacement of the hemilabile phosphine oxide occurs, followed by ligand rotation, to open a coordination site on palladium. After addition of the imidazole **2**, the CMD process occurs via a six-membered transition-state in which the pivalate plays a key role, producing the biaryl palladium complex. Ligand rotation to an inner sphere orientation precedes PivOH displacement to give a complex ready for reductive elimination to afford the cross-coupled product **3**.

While intermediate **I·Br** is isolable when prepared under stoichiometric conditions at ambient temperature, the kinetic finding that the reaction is zero-order in [KOPiv], and the

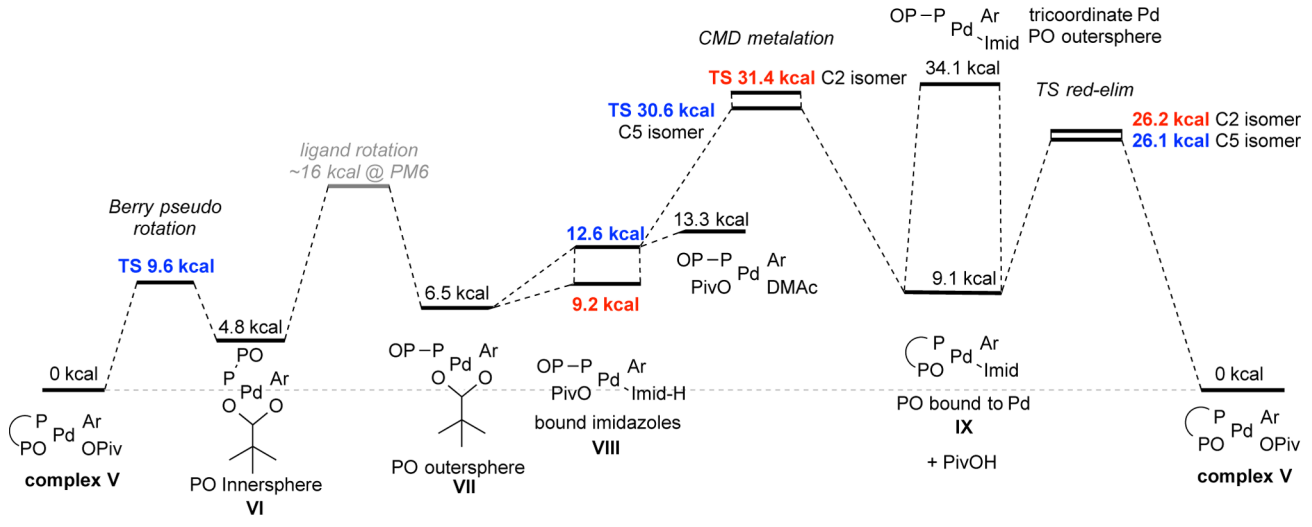

Figure 15. Reaction coordinate (thermal free energy profile) for the coupling of pyrrole **1** to imidazole **2** mediated by Pd·xantphos(O). The represented energies (kcal mol^{-1}) are relative to the oxidative addition complex **V**. Calculations were done using B3LYP/defSV(P) and ECP on heavy elements (Pd). Energy levels shown are representative and not to scale.

DOI: 10.1021/jacs.5b01913
J. Am. Chem. Soc. 2015, 137, 13272−13281

Scheme 7. Proposed Mechanism for the Reaction of Scheme 1 Highlighting Critical Species and Kinetically Meaningful Steps Defined by the Experimental and Computational Results

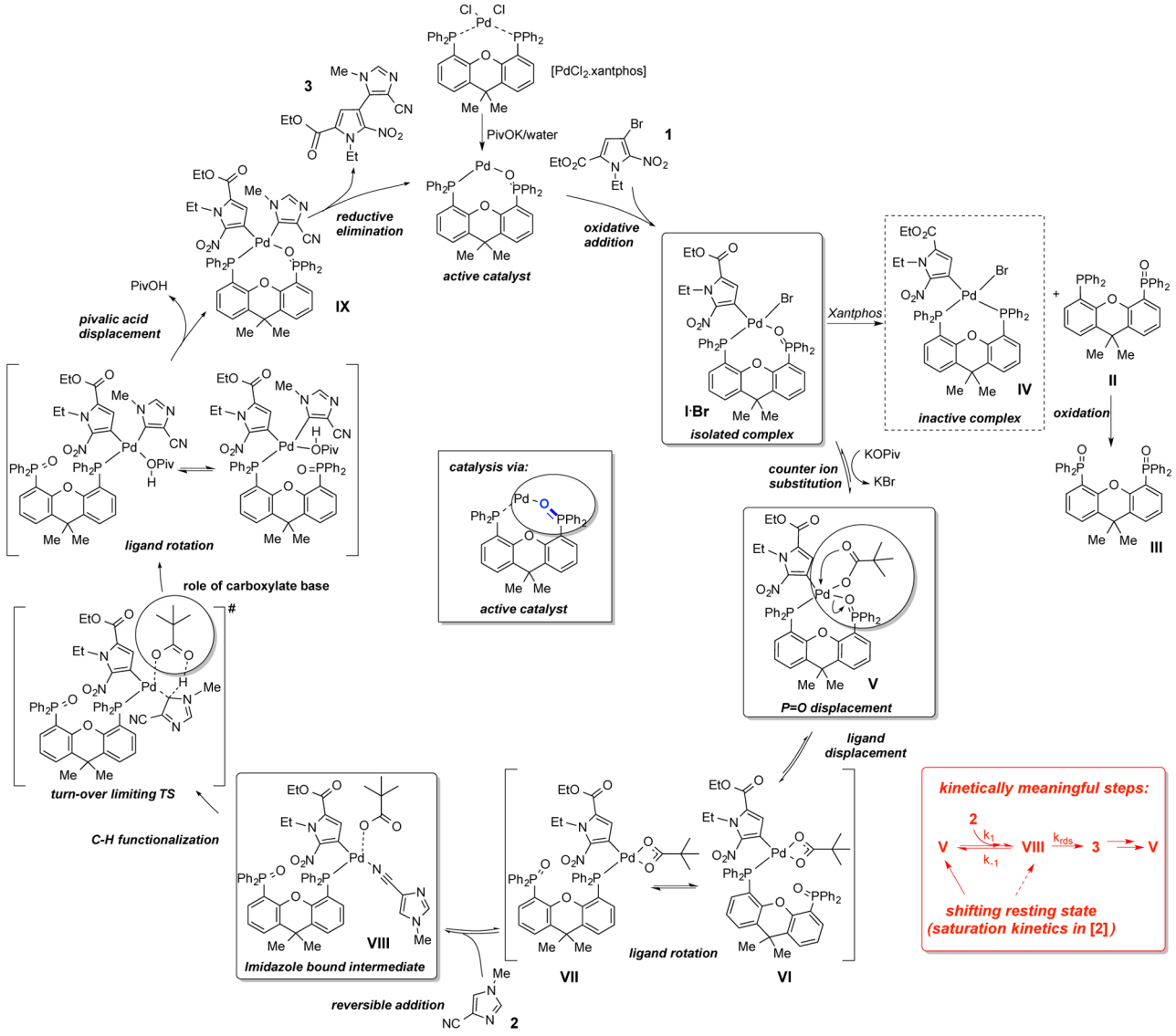

NMR results showing changes upon KOPiv addition to **I·Br** suggest that in the catalytic network, ion exchange with pivalate to form species **V** is facile[29] and that this species dominates under reaction conditions. Thus, the kinetically meaningful steps, as defined by the experimental results and supported by the computational reaction coordinate shown in Figure 15, are highlighted in the red box in Scheme 7. The steady-state catalytic rate law, derived assuming the total catalyst in the active cycle is partitioned between species **V** and **VIII**, is given by eq 2 (see Supporting Information for derivation). At high concentrations of **2**, the reaction exhibits zero-order kinetics in both substrates, as observed in the experimental kinetic profiles.

$$\text{rate} = \frac{k_1 k_{\text{rds}}[\mathbf{2}][\text{cat}]_{\text{total}}}{k_{-1} + k_{\text{rds}} + k_1[\mathbf{2}]} \qquad (2)$$

Generality. The experimental and theoretical results highlight the role of the hemilabile monophosphine oxide both in catalyst activation as well as in the catalytic cycle, leading to the question of whether mono-oxides of bidentate phosphine ligands form generally in related Pd(II) mediated reactions. Several other systems were tested to probe this phenomenon, including the Suzuki reaction shown in Scheme 8 using $Pd(OAc)_2$/BINAP. NMR studies show that the ligand complexes to Pd(II) in the presence of aqueous base and ArBr to form the Pd(II) oxidative addition adduct shown, accompanied by mono-oxidation of the

Scheme 8. Observation of Mono-phosphine Oxide Complex in Catalyst Activation of a Suzuki Coupling Reaction

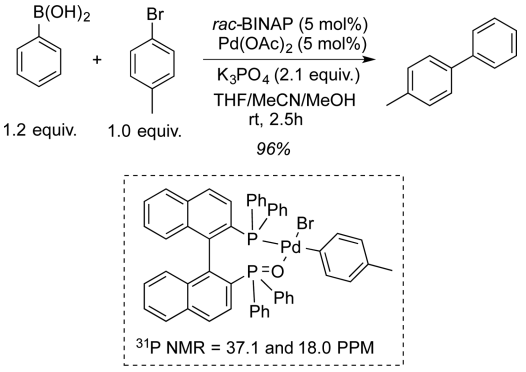

DOI: 10.1021/jacs.5b01913
J. Am. Chem. Soc. 2015, 137, 13272−13281

bidentate phosphine. This catalyst was highly active in the Suzuki process with $PhB(OH)_2$, with the reaction going to completion in only 2.5 h at room temperature. Similar results were found for the same reaction using $PdCl_2$·xantphos as well as in several other coupling reactions (see Supporting Information). These additional examples lend support to the suggestion that the formation of bidentate phosphine mono-oxides may be a more general phenomenon when Pd(II) precatalysts are used in coupling processes. Expansion of this motif to other bis-phosphine ligands in other reactions following a similar mechanism is currently a major focus of our work.

CONCLUSIONS

In summary, we have identified the previously unknown Pd-xantphos mono-oxide complex, which is the catalytically active species in a palladium-mediated direct C−H arylation, and we have isolated its oxidative addition complex with the pyrrole substrate in the reaction of Scheme 1. The rapid in situ formation of the active catalyst under reaction conditions prior to oxidative addition suggests that such a catalyst may be active in related coupling reactions. Indeed, similar species, with several different bidentate phosphines, have been implicated in other coupling processes.

In the present coupling, the importance of phosphine oxidation to the successful transformation was elucidated, along with understanding the inhibiting role of excess phosphine. These studies should prove general, due to the common use of similar conditions (i.e., bidentate ligand, Pd(II) precatalyst in the presence of base and water) in a variety of coupling processes. This work shows that the importance of the phosphine oxidation is twofold: (1) the mono-oxide of the bis-phosphine enables a bidentate ligand to function in this reaction; and (2) the hemilabile nature of the ligand presumably increases the stability of the Pd(0) center postreductive elimination but prior to the next oxidative addition. A similar role of monodentate phosphine oxides has been previously proposed.[44]

A dual role for the carboxylate base was proposed: first in aiding the formation of the active phosphine mono-oxide catalyst, and second in functioning as the locus of proton abstraction in the CMD transition state. In neither role does the concentration of the base influence reaction rate, while its structure appears to be critical in the latter role.

Navigating the influence of catalyst activation on the structure of the active catalyst in coupling reactions significantly impacts our ability to implement challenging coupling processes. The results disclosed herein may lead to the design of better coupling processes in a general setting where catalyst structure and reactivity of bidentate phosphine ligands may be influenced by phosphine oxidation.

ASSOCIATED CONTENT

Supporting Information

The Supporting Information is available free of charge on the ACS Publications website at DOI: 10.1021/jacs.5b01913.

Full experimental details, spectroscopic data, X-ray data, supplementary experiments (PDF)

AUTHOR INFORMATION

Corresponding Authors

*Blackmond@scripps.edu
*martin.eastgate@bms.com

Notes

The authors declare no competing financial interest.

ACKNOWLEDGMENTS

This work was supported by the BMS-Scripps collaboration and by the NSF Centers for Chemical Innovation: Center for Catalytic C−H Functionalization (CCHF, CHE-0943980). The authors are grateful for helpful advice on the NMR spectroscopy from D. Huang and L. Paternack and for crystallography from Curtis Moore and Arnold Rheinhold (UCSD). The authors would like to thank Drs. David Kronenthal, Rajendra Deshpande, Rodney Parsons and Ke Chen for supporting this work, Antonio Ramirez and Gregory Beutner for useful discussions. We would also like to thank Lopa Desai and Neil Strotman for initial screening which identified this coupling process.

REFERENCES

(1) (a) Ishiyama, T.; Murata, M.; Miyaura, N. *J. Org. Chem.* **1995**, *60*, 7508. (b) Cho, J.-Y.; Tse, M. K.; Holmes, D.; Maleczka, R. E., Jr.; Smith, M. R., III *Science* **2002**, *295*, 305. (c) Molander, G. A.; Cavalcanti, L. N.; García-García, C. *J. Org. Chem.* **2013**, *78*, 6427.

(2) (a) Percec, V.; Golding, G. M.; Smidrkal, J.; Weichold, O. *J. Org. Chem.* **2004**, *69*, 3447. (b) Lu, Y.; Plocher, E.; Hu, Q.-S. *Adv. Synth. Catal.* **2006**, *348*, 841. (c) Shang, R.; Ilies, L.; Asako, S.; Nakamura, L. *J. Am. Chem. Soc.* **2014**, *136*, 14349.

(3) (a) Pascual, S.; Mendoza, P.; Braga, A. C. C.; Maseras, F.; Echavarren, A. M. *Tetrahedron* **2008**, *64*, 6021. (b) Huang, J.; Chan, J.; Chen, Y.; Borths, C. J.; Baucom, K. D.; Larsen, R. D.; Faul, M. M. *J. Am. Chem. Soc.* **2010**, *132*, 3674.

(4) (a) Hamann, B. C.; Hartwig, J. F. *J. Am. Chem. Soc.* **1998**, *120*, 7369. (b) Hamann, B. C.; Hartwig, J. F. *J. Am. Chem. Soc.* **1998**, *120*, 3694. (c) Ogasawara, M.; Yoshida, K.; Hayashi, T. *Organometallics* **2000**, *19*, 1567. (d) Klingensmith, L. M.; Strieter, E. R.; Barder, T. E.; Buchwald, S. L. *Organometallics* **2006**, *25*, 82. (e) Ngassa, F. N.; DeKorver, K. A.; Melistas, T. S.; Yeh, E. A.-H.; Lakshman, M. K. *Org. Lett.* **2006**, *8*, 4613. (f) Hamid, M. H. S. A.; Williams, J. M. J. *Chem. Commun.* **2007**, 725. (g) Daniels, D. S. B.; Jones, A. S.; Thompson, A. L.; Paton, R. S.; Anderson, E. A. *Angew. Chem., Int. Ed.* **2014**, *53*, 1915. (h) Vidadala, S. R.; Golz, C.; Strohmann, C.; Daniliuc, C.-G.; Waldmann, H. *Angew. Chem., Int. Ed.* **2014**, *53*, 651.

(5) (a) Cabri, W.; Candiani, I.; Bedeschi, A. *J. Org. Chem.* **1992**, *57*, 3558. (b) McConville, M.; Saidi, O.; Blacker, J.; Xiao, J. *J. Org. Chem.* **2009**, *74*, 2692. (c) Oyamada, J.; Kitamura, T. *Chem. Commun.* **2008**, 4992. (d) Qin, L.; Hirao, H.; Zhou, J. (S.) *Chem. Commun.* **2013**, *49*, 10236. (e) Feng, Z.; Min, Q.-Q.; Zhao, H.-Y.; Gu, J.-W.; Zhang, X. *Angew. Chem., Int. Ed.* **2015**, *54*, 1270.

(6) Boezio, A. A.; Pytkowicz; Cote, A.; Charette, A. B. *J. Am. Chem. Soc.* **2003**, *125*, 14260.

(7) Carrow, B. P.; Nozaki, K. *J. Am. Chem. Soc.* **2012**, *134*, 8802.

(8) Desrosiers, J.-N.; Charette, A. B. *Angew. Chem., Int. Ed.* **2007**, *46*, 5955.

(9) Cote, A.; Lindsay, V. N. G.; Charette, A. B. *Org. Lett.* **2007**, *9*, 85.

(10) Wu, C.; Zhou, J. (S). *J. Am. Chem. Soc.* **2014**, *136*, 650.

(11) Wei, C. S.; Davies, G. H. M.; Soltani, O.; Albrecht, J.; Gao, Q.; Pathirana, C.; Hsiao, Y.; Tummala, S.; Eastgate, M. D. *Angew. Chem., Int. Ed.* **2013**, *52*, 5822.

(12) (a) Hillebrand, S.; Bruckmann, J.; Kruger, C.; Haenel, M. W. *Tetrahedron Lett.* **1995**, *36*, 75. (b) Kranenburg, M.; van der Burgt, Y. E. M.; Kamer, P. C. J.; van Leeuwn, P. W. N. M. *Organometallics* **1995**, *14*, 3081.

(13) (a) Davies, D. L.; Donald, S. M. A.; Al-Duaij, O.; Macgregor, S. A.; Polleth, M. *J. Am. Chem. Soc.* **2006**, *128*, 4210. (b) Garcia-Cuadrado, D.; Braga, A. C. C.; Maseras, F.; Echavarren, A. M. *J. Am. Chem. Soc.* **2006**, *128*, 1066. (c) Ackermann, L.; Vicente, R.; Althammaer, A. *Org. Lett.* **2008**, *10*, 2299. (d) Fagnou, K. *Top. Curr. Chem.* **2009**, *292*, 35.

DOI: 10.1021/jacs.5b01913
J. Am. Chem. Soc. 2015, 137, 13272−13281

(14) (a) Pivsa-Art, S.; Satoh, T.; Kawamura, Y.; Miura, M.; Nomura, M. *Bull. Chem. Soc. Jpn.* **1998**, *71*, 467. (b) Bellina, F.; Cauteruccio, S.; Mannina, L.; Rossi, R.; Viel, S. *J. Org. Chem.* **2005**, *70*, 3997. (c) Satoh, T.; Miura, M. *Chem. Lett.* **2007**, *36* (2), 200. (d) Chiong, H. A.; Daugulis, O. *Org. Lett.* **2007**, *9*, 1449. (e) Chuprakov, S.; Chernyak, N.; Dudnik, A. S.; Gevorgyan, V. *Org. Lett.* **2007**, *9*, 2333.
(15) (a) Biswas, B.; Sugimoto, M.; Sakaki, S. *Organometallics* **2000**, *19*, 3895. (b) Davies, D. L.; Donald, S. M. A.; Macgregor, S. A. *J. Am. Chem. Soc.* **2005**, *127*, 13754. (e) Garcia-Cuadrado, D.; de Mendoza, P.; Braga, A. C. C.; Maseras, F.; Echavarren, A. M. *J. Am. Chem. Soc.* **2007**, *129*, 6880. (f) Lapointe, D.; Fagnou, K. *Chem. Lett.* **2010**, *39*, 1118.
(16) (a) González, J. J.; García, N.; Gómez-Lor, B.; Echavarren, A. M. *J. Org. Chem.* **1997**, *62*, 1286. (b) Hennessy, E. J.; Buchwald, S. L. *J. Am. Chem. Soc.* **2003**, *125*, 12084. (c) Gómez-Lor, B.; Echavarren, A. M. *Org. Lett.* **2004**, *6*, 2993. (d) Campeau, L.-C.; Parisien, M.; Leblanc, M.; Fagnou, K. *J. Am. Chem. Soc.* **2004**, *126*, 9186. (e) Campeau, L.-C.; Parisien, M.; Jean, A.; Fagnou, K. *J. Am. Chem. Soc.* **2006**, *128*, 581. (f) Lafrance, M.; Rowley, C. N.; Woo, T. K.; Fagnou, K. *J. Am. Chem. Soc.* **2006**, *128*, 8754.
(17) (a) Lafrance, M.; Fagnou, K. *J. Am. Chem. Soc.* **2006**, *128*, 16496. (b) Lafrance, M.; Lapointe, D.; Fagnou, K. *Tetrahedron* **2008**, *64*, 6015. (c) Benoit Liégault, B.; Lapointe, D.; Caron, L.; Vlassova, A.; Fagnou, K. *J. Org. Chem.* **2009**, *74*, 1826.
(18) (a) Blackmond, D. G. *Angew. Chem., Int. Ed.* **2005**, *44*, 4302. (b) Mathew, J. S.; Klussmann, M.; Iwamura, H.; Valera, F.; Futran, A.; Emanuelsson, E. A. C.; Blackmond, D. G. *J. Org. Chem.* **2006**, *71*, 4711.
(19) In these experiments, a series of reactions are monitored using the same initial concentration of one substrate while varying the initial concentration of the other.
(20) Hall, S. R.; Skelton, B. W.; White, A. H. *Aust. J. Chem.* **1983**, *36*, 267.
(21) Ebrahim, M.; Neels, A.; Stoeckli-Evans, H.; Panchanatheswaran, K. M. *Polyhedron* **2007**, *26*, 1277.
(22) Bakar, M. A.; Hills, A.; Hughes, D. L.; Leigh, G. J. *J. Chem. Soc., Dalton Trans.* **1989**, 1417.
(23) Saravanabharathi, D.; Nethaji, M.; Samuelson, A. G. *Polyhedron* **2002**, *21*, 2793.
(24) (a) Farrer, N. J.; McDonnald, R.; Piga, T.; McIndole, J. S. *Polyhedron* **2010**, *29*, 254. (b) Sgarbossa, P.; Pizzo, E.; Scarso, A.; Sbovata, S. M.; Michelin, R. A.; Mozzon, M.; Strukul, G.; Benetollo, F. *J. Organomet. Chem.* **2006**, *691*, 3659.
(25) Faller, J. W.; Parr, J. *Organometallics* **2000**, *19*, 3556.
(26) Zhang, Y.; Ding, Y.; Pullarkat, S. A.; Li, L.; Leung, P.-H. *J. Organomet. Chem.* **2011**, *696*, 709.
(27) A sample of xantphos mono-oxide was prepared by the catalytic mono-oxidation procedure reported by Grushin and workers. (a) Grushin, V. V. *J. Am. Chem. Soc.* **1999**, *121*, 5831. (b) Grushin, V. V. *Organometallics* **2001**, *20*, 3950. (c) Grushin, V. V. *Chem. Rev.* **2004**, *104*, 1629.
(28) (a) Ioele, M.; Ortaggi, G.; Scarsella, M.; Sleiter, G. *Polyhedron* **1991**, *10*, 2475. (b) Amatore, C.; Jutand, A.; M'Barki, M. A. *Organometallics* **1992**, *11*, 3009. (c) Grushin, V. V.; Alper, H. *Organometallics* **1993**, *12*, 1890. (d) Grushin, V. V.; Bensimon, C.; Alper, H. *Inorg. Chem.* **1994**, *33*, 4804. (e) Amatore, C.; Carré, E.; Jutand, A.; M'Barki, M. A. *Organometallics* **1995**, *14*, 1818. (f) Amatore, C.; Carré, E.; Jutand, A.; M'Barki, M. A.; Meyer, G. *Organometallics* **1995**, *14*, 5605. (g) Csákai, Z.; Skoda-Földes, R.; Kollár, L. *Inorg. Chim. Acta* **1999**, *286*, 93. (h) Amatore, C.; Jutand, A. *Acc. Chem. Res.* **2000**, *33*, 314.
(29) (a) Morehouse, S. M.; Powell, A. R.; Heffer, J. P.; Stephenson, T. A.; Wilkinson, G. *Chem. Ind. (London)* **1964**, 544. (b) Stephenson, T. A.; Morehouse, S. M.; Powell, A. R.; Heffer, J. P.; Wilkinson, G. *J. Chem. Soc.* **1965**, 3632. (c) Tan, Y.; Hartwig, J. F. *J. Am. Chem. Soc.* **2011**, *133*, 3308.
(30) (a) Simmons, E. M.; Hartwig, J. F. *Angew. Chem., Int. Ed.* **2012**, *51*, 3066.
(31) Frisch, M. J.; Trucks, G. W.; Schlegel, H. B.; Scuseria, G. E.; Robb, M. A.; Cheeseman, J. R.; Scalmani, G.; Barone, V.; Mennucci, B.; Petersson, G. A.; Nakatsuji, H.; Caricato, M.; Li, X.; Hratchian, H. P.; Izmaylov, A. F.; Bloino, J.; Zheng, G.; Sonnenberg, J. L.; Hada, M.; Ehara, M.; Toyota, K.; Fukuda, R.; Hasegawa, J.; Ishida, M.; Nakajima, T.; Honda, Y.; Kitao, O.; Nakai, H.; Vreven, T.; Montgomery, J. A., Jr.; Peralta, J. E.; Ogliaro, F.; Bearpark, M.; Heyd, J. J.; Brothers, E.; Kudin, K. N.; Staroverov, V. N.; Kobayashi, R.; Normand, J.; Raghavachari, K.; Rendell, A.; Burant, J. C.; Iyengar, S. S.; Tomasi, J.; Cossi, M.; Rega, N.; Millam, M. J.; Klene, M.; Knox, J. E.; Cross, J. B.; Bakken, V.; Adamo, C.; Jaramillo, J.; Gomperts, R.; Stratmann, R. E.; Yazyev, O.; Austin, A. J.; Cammi, R.; Pomelli, C.; Ochterski, J. W.; Martin, R. L.; Morokuma, K.; Zakrzewski, V. G.; Voth, G. A.; Salvador, P.; Dannenberg, J. J.; Dapprich, S.; Daniels, A. D.; Farkas, Ö.; Foresman, J. B.; Ortiz, J. V.; Cioslowski, J.; Fox, D. J. *Gaussian*; Gaussian, Inc.; Wallingford, CT, 2009.
(32) defSV(P): Weigend, F.; Ahlrichs, R. *Phys. Chem. Chem. Phys.* **2005**, *7*, 3297.
(33) Basis set obtained from EMSL Basis Set Exchange Library.
(34) Zhao, Y.; Truhlar, D. G. *J. Chem. Theory Comput.* **2009**, *5*, 324.
(35) Godbout, N.; Salahub, D. R.; Andzelm, J.; Wimmer, E. *Can. J. Chem.* **1992**, *70*, 560.
(36) (a) Stevens, W. J.; Basch, H.; Krauss, M. *J. Chem. Phys.* **1984**, *81*, 6026. (b) Stevens, W. J.; Krauss, M.; Basch, H.; Jasien, P. G. *Can. J. Chem.* **1992**, *70*, 612.
(37) Available through Gaussian.
(38) Bonnaventure, I.; Charette, A. B. *J. Org. Chem.* **2008**, *73*, 6330.
(39) Berry, R. S. *J. Chem. Phys.* **1960**, *32*, 933.
(40) Lapointe, D.; Fagnou, K. *Chem. Lett.* **2010**, *39*, 1118 for an overview of mechanistic studies of the CMD mechanism..
(41) The bis-aryl side product (the result of both C2 and C5 arylation on the imidazole) is believed to be the result of C5 arylation of the C2-product, which serves to increase the observed selectivity (>50:1) vs the inherent selectivity of the catalyst system. Thus, the calculated transition-state energy difference between direct C2 and C5 arylation would be expected to be closer to 1 kcal mol^{-1}.
(42) (a) Gorelsky, S. I.; Lapointe, D.; Fagnou, K. *J. Org. Chem.* **2012**, *77*, 658. (b) Gorelsky, S. I.; Lapointe, D.; Fagnou, K. *J. Am. Chem. Soc.* **2008**, *130*, 10848.
(43) Pudasaini, B.; Janesko, B. G. *Organometallics* **2011**, *30*, 4564.
(44) Denmark, S. E.; Smith, R. C.; Tymonko, S. A. *Tetrahedron* **2007**, *63*, 5730.

DOI: 10.1021/jacs.5b01913
J. Am. Chem. Soc. 2015, 137, 13272−13281